RESEARCH PAPER

Experimental Investigation of Vertical Bearing Characteristics of Composite Post-grouting Piles in Sandy Soil

Shuai Cao[1] · Qinke Wang[2] · Jianlin Ma[1] · Zili Xiao[3] · Chaoyi Li[1] · Yanxin Yang[4] · Jun Wang[5]

Abstract

As a novel technology for strengthening the bearing capacity of bridge piles, related research on composite post-grouting at pile ends is still underdeveloped. To reveal the reinforcement mechanism and bearing characteristics of composite post-grouting piles, indoor model tests were implemented in sandy soil, which applied different grouting methods, including non-grouting, open post-grouting, and composite post-grouting methods on three pile-ends, and static load compression tests were conducted. The load–settlement curves, grouting curing performance, axial force of the pile, frictional resistance of the pile side, pile-soil relative displacement, and pile-end resistance were compared and investigated. The experimental results show that the load–settlement curves indicated the same pattern of steep variation. Compared to the pile without grouting, the ultimate compressive bearing capacity of the model pile was improved by 67.2% and 101.6% using the open post-grouting and composite post-grouting methods at the pile end, respectively. Compared to S1 pile without grouting, the average frictional resistance of the pile side in the slurry up-return zones under the ultimate condition for S2 (open post-grouting) and S3 (composite post-grouting) increased by 109.3% and 129.3%, respectively. In contrast, the pile-end resistance increased 2.3 times and 2.9 times, respectively. Therefore, the bearing capability of piles can be improved more effectively when using the composite post-grouting technique in sandy soil rather than the traditional open post-grouting technique. These findings can be used as references for the optimized design and application of composite post-grouting bridge-pile foundations.

Keywords Sandy soil · Composite post-grouting · Model pile · Bearing characteristics · Indoor model test

✉ Qinke Wang
qkwang_90@163.com

Shuai Cao
cs@my.swjtu.edu.cn

Jianlin Ma
majianlin01@126.com

Zili Xiao
386446683@qq.com

Chaoyi Li
784012903@qq.com

Yanxin Yang
yanxinyangswjtu@foxmail.com

Jun Wang
632790186@qq.com

[1] School of Civil Engineering, Southwest Jiaotong University, Chengdu 610031, China

[2] School of Civil Engineering and Architecture, Southwest University of Science and Technology, Mianyang 621010, China

[3] Chengdu Rail Transit Group Co., Ltd., Chengdu 610041, China

[4] School of Civil Engineering, Sichuan University of Science and Engineering, Zigong 643000, China

[5] Sichuan Province Airport Group Co., Ltd., Chengdu 610202, China

1 Introduction

A large number of bridge projects have been applied in the construction of high-speed railways in China; for example, the total length of the bridge section of the Beijing-Shanghai high-speed railway accounts for more than 80% of the total line length. Bored piles with mud retaining walls are widely adopted during the construction of bridge foundations, and have the benefits of high stiffness, high bearing capacity, small pile deformation, and effective control of bridge settlement deformation [1, 2]. However, bored piles with mud retaining walls have disadvantages such as significant disturbance in soil and residual silt at the pile end, which will further reduce the pile tip resistance [3–5]. Many studies have shown that post-grouting technology of pile foundations can effectively improve the shortcomings mentioned above [6–8], and open post-grouting technology is the most commonly used. However, open post-grouting has low controllability and is prone to flow along soil fissures under high pressure [9]. To address this issue, a new type of composite post-grouting technology at the pile tip improves the previous open post-grouting technology. Its main characteristics are the installation of a hollow steel plate capsule closed post grouting device and a common open post grouting pipe at the bottom of the pile. After the pile was formed, a three-step post grouting process of "open closed open" was used to compact, penetrate, and split the surrounding sediment and disturbed strata of the pile bottom. The slurry is pressed into a hollow steel plate capsule to expand and form an enlarged head at the pile end, expanding the supporting area of the pile, and compacting and consolidating the soil around the pile end [9]. Therefore, the pile-end composite post-grouting technology can effectively control the area, pressure, and volume of grouting, improve the pile-bearing capacity, and reduce the settlement volume. A grouting performance comparison diagram of the open and composite post-grouting pile ends is shown in Fig. 1. Therefore, investigations on the bearing characteristics and reinforcement mechanism of composite post-grouting piles are vital and have essential engineering significance and scientific value for developing high-speed railways in China.

The application of post-pressure grouting technology has been investigated in many studies. For example, Bruce [10] summarized the construction process and test results of bored piles that used the post-grouting technique and outlined the influences of post-grouting on the bearing capacity and settlement of bored piles. Sherwood and Mitchell [11] presented a comparative test between piles with or without grouting. They suggested that grouting reduces the settlement and improves the stiffness of the soil at the pile end by improving the mechanical properties of the disturbed soil. Ruiz and Pando [12] indicated that the primary reinforcement mechanism for the bearing capacity improvement of pile foundations is soil enhancement achieved by pile-end grouting, and the reinforcement mechanism was verified using modified load transfer curves. Thiyyakkandi [13] carried out model tests of post-grouting of monopiles and multi-piles at the pile ends in cohesionless soil, in which the model foundations were excavated and the post-compaction piles were removed after the tests to analyze the shape and size of the slurry bubbles. Thiyyakkandi et al. [14] used PLAXIS 2D software to simulate the entire experimental process of jetted and grouted precast piles and proposed a method to obtain the load–displacement response of piles in cohesionless soil. Nguyen and Fellenius [7] conducted static load tests on the pile-side of grouting piles in a high-rise building in Vietnam, which have different pile diameter including 1.5 m and 2.0 m. It was found that the pile-side grouting piles increased the lateral frictional resistance by two to three times compared to the non-grouting piles. Youn and Tonon [15] investigated the influences of post-grouting on the bearing capacity of bored piles based on field experiments and numerical simulations. The results indicated that the negative frictional resistance caused by the pre-pressure of the pile end enhances the pile-side frictional resistance. Fang et al. [16] reported that the pre-pressure of the post-grouting pile at the pile end effectively increased the frictional resistance of the pile end and pile side, which has been confirmed by many field cases. Xu et al. [17] conducted post-grouting tests on bored piles in karst areas, proposing a mathematical model to investigate the grouting pressure and water cement ratio. Compared to the conventional pile, there are 1.5 times higher bearing capacity and 50% lower settlement when using the membrane-confined grouted pile. Wan et al. [18] conducted post-grouting field tests on bridge pile foundations in fine sand layers, and the EWCT technique and standard penetration tests were used to measure the reinforcement of post-grouting.

The above literature shows that open post-grouting technology has been widely studied and applied. However, the open post-grouting method has disadvantages such as poor grouting performance, rugged construction, and poor stability of load-bearing capacity improvement. Composite post-grouting technology can avoid these barriers and has the advantages of open post-grouting technology. As described earlier, the influence of composite post-grouting technology on the bearing characteristics and reinforcement mechanism of pile foundations has not been deeply understood. In this study, the laboratory model tests were implemented in sandy soil, which applied different grouting methods, including non-grouting, open post-grouting, and composite post-grouting on three pile ends, and static
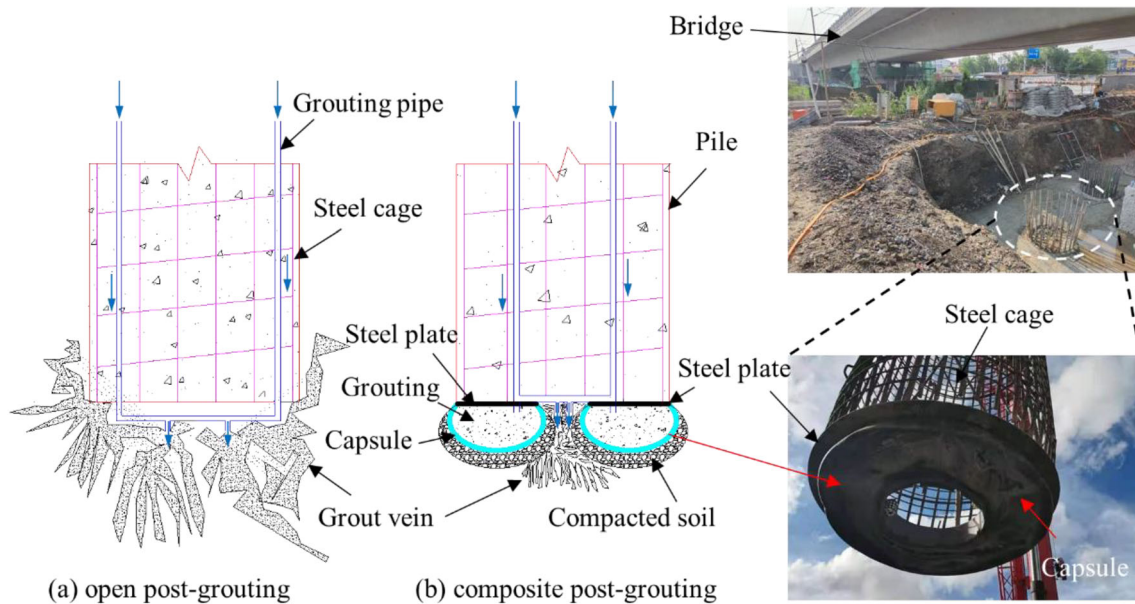
Fig. 1 Comparison of pile-ends grouting performance between open and composite post-grouting methods

load compression tests were conducted. The load–settlement curves, slurry curing effect, pile axial force, pile-side frictional resistance, pile-soil relative displacement, and pile-end resistance characteristics were compared. These results provide a scientific basis for the promotion of composite post-grouting technology in bridge pile foundation engineering.

2 Experimental Program

2.1 Similarity Relationship

To ensure similarity with on-site tests, model tests can be satisfied through two similarity principles: mechanical similarity and geometric similarity. Mechanical similarity consists of material strength similarity (compressive strength, etc.), material stress similarity (stress, strain, etc.), elastic similarity (elastic modulus, displacement, etc.), and mechanical characteristic similarity of the test soil (cohesion, internal friction angle, etc.). Geometric similarity determines the size of the model test according to a certain proportional relationship. However, for the soil and structure in the 1-g model test, it is difficult to perfectly follow similar laws [19]. According to the site prototype pile diameter of 1.0 m and Buckingham's similarity theory [20], the mechanical similarity constant (model/prototype) is 1:1, and the geometric similarity constant (model/prototype) is 1:10 for the selected model test.

2.2 Experimental Setup and Equipment

Figure 2 shows the setup and equipment for the model test. The test devices included a container, loading system, grouting system, data logger, and measuring instruments. The container of dimension of 0.9 m × 0.9 m × 2.5 m (representing length × width × height), and the container is welded with a steel plate of 5 mm thickness, which can maintain the overall stability during the test. The loading system mainly consists of a hydraulic jack, two YHD-200 displacement meters, a loading beam, and other components. The loading beam was fixed on the counter-force rack as a support to provide a vertical force for the model pile by applying downward pressure. A hydraulic jack is installed between the loading beam and the model pile to apply downward axial pressure to the pile, and the variations in pile-top load are recorded in real time by the pressure sensor. During the loading process, two YHD-200 displacement meters were used to monitor the pile top settlement with each load, which is applicable with a displacement within 200 mm and an accuracy of 0.01 mm.

The post-grouting system consisted of an air compressor and a cement slurry tank, as shown in Fig. 3. The air compressor provides a maximum grouting pressure of 0.8 MPa for the model pile to be reinforced after installation. The cement slurry tank is a cylinder with a diameter of 0.4 m and height of 0.4 m. The cement slurry tank is made of a steel plate, in which the wall thickness is 5 mm and the top plate thickness is 10 mm. Moreover, the top plate of the cement slurry tank is connected to the tank body by high-strength bolts, with a rubber ring between the top plate and the tank body to ensure airtightness and an air
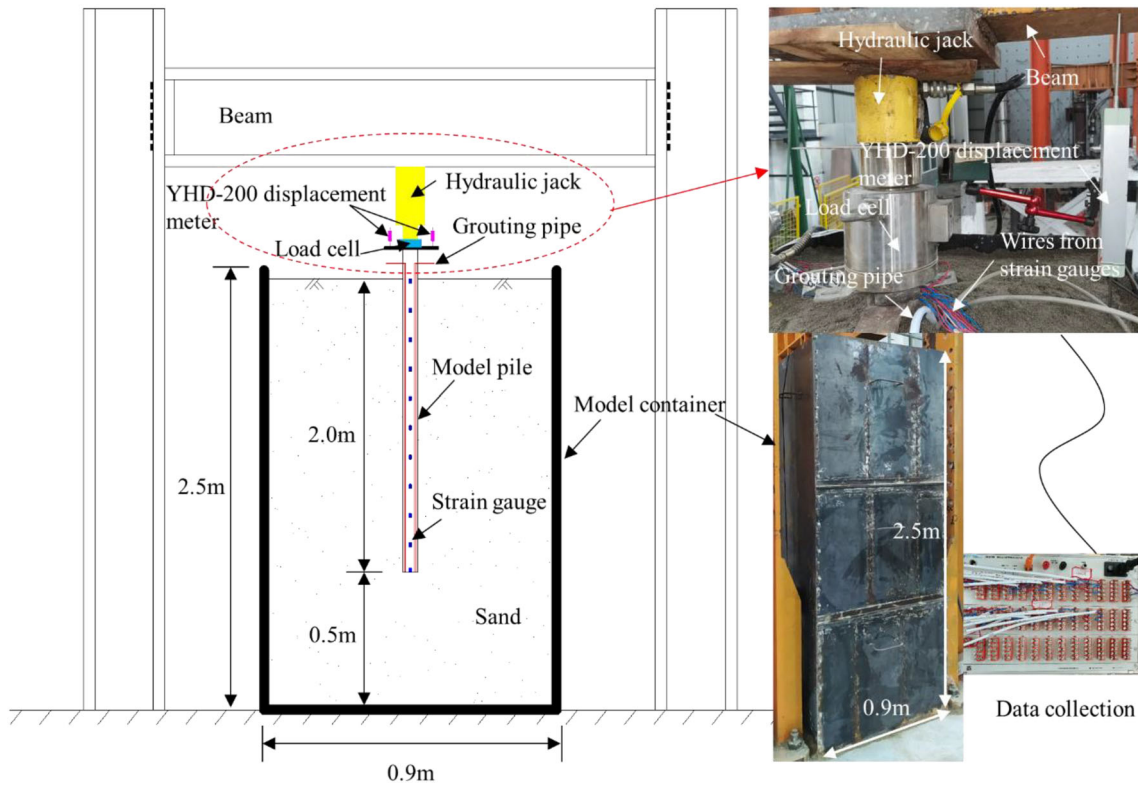
Fig. 2 The schematic and pictures of model test set-up
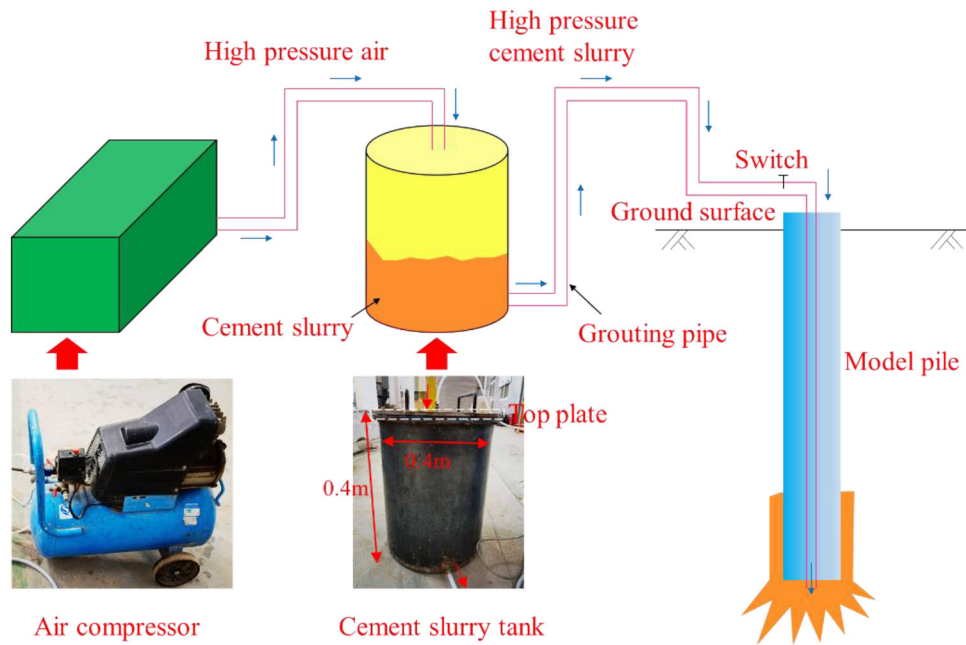

Fig. 3 Post-grouting equipment

inlet on the top plate. The air compressor provides high-pressure air into the hydraulic cement slurry tank through the air inlet pipe, and the cement slurry inside is injected into the pile end through the cement slurry outlet pipe.

2.3 Sandy Soil

In this study, because the bearing layer of the prototype pile end is a sandy soil layer, the natural river sand of the

Jinsha River Basin with a particle size distribution curve similar to that of the prototype sand was selected for the test. Before preparing the physical model, the main mechanical parameters of sand were ensured to meet the mechanical similarity through testing. The foundation in the container is made of 2.5 m sandy soil. The properties of the sandy soil obtained through a series of indoor tests are listed in Table 1. The influence of grain size on the pile-soil interaction should be considered in the 1-g model tests. To investigate the response of piles subjected to lateral loading, Garnier et al. [21] recommended that the diameter ratio of the pile (D_m) to the median soil grain (D_{50}) should be larger than 60, thereby minimizing the effect of grain size. Moreover, Craig [22] pointed out that the grain size is insufficient to affect the bearing capacity of the foundations when the structural size of the model is greater than 40 times the grain size. It can be seen from Fig. 4 that 98% of the particle size selected for this test is less than 1.9 mm, and the median soil particle diameter (D_{50}) is 0.45 mm. Therefore, the effect of the particle size of the model foundation material on the bearing performance of the monopile in this study can be ignored ($100/0.45 > 60$ and $100/1.9 > 40$).

2.4 Model Pile

The model pile consisted of a reinforcement cage and concrete. The pile's diameter is 0.1 m and its length is 2.05 m, as shown in Fig. 5. The reinforcement cage was made of six steel bars of 8 mm diameter and 2.0 m length as the primary reinforcement, with 2 mm diameter iron wire as the hoop reinforcement, and the longitudinal spacing was arranged at 0.2 m. The distance between the container's inner side wall and the test pile should be
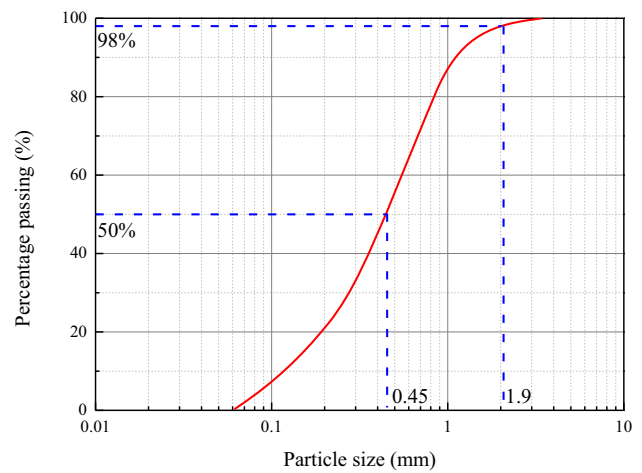
Table 1 Physical properties of sand

Property	Unit	Value
Unit weight	kN/m^3	18.2
Specific gravity	\	2.64
Minimum void ratio	\	0.559
Maximum void ratio	\	0.873
Void ratio	\	0.604
Relative density	%	85.7
Water content	%	10.6
Compression modulus	MPa	11.8
Elastic modulus	MPa	20.2
Poisson's ratio	\	0.3
Internal friction angle	°	32.4
Cohesion	kPa	0.1

Fig. 4 Particle size distribution curve
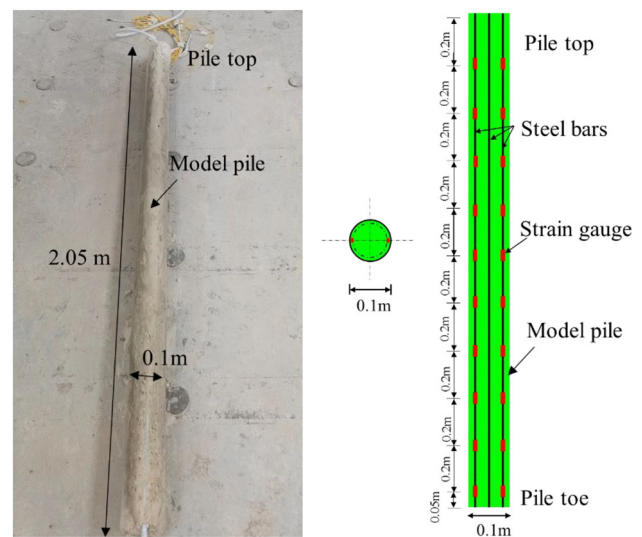
Fig. 5 Photograph of piles and layout of strain gauges

greater than 2.82 times the pile's diameter d [23]. The distance between the model pile and container wall in this study is $9d$ (90 cm/10 cm = 9), and the boundary effect can be eliminated. The reinforcement cage was fixed in a PVC mold with a closed end and a diameter of 10 cm. C30 concrete, which has 30 MPa compressive strength of cube specimens with a 150 mm length, was poured into the mold, vibrated, and compacted. It is noteworthy that the test pile was filled with C30 concrete, with a mix ratio of water: cement: sand: crushed stone = 0.38:1:1.11:2.72. After 7 days of maintenance, the PVC mold was removed and maintained for another 28 days, and the weight of the model pile was determined to be 25 kN/m^3, the elastic modulus was 3.0 GPa, and the Poisson's ratio was 0.2. Three model piles were used in the experimental work, including non-grouting (denoted as S1), open-grouting (denoted as S2), and composite-grouting (denoted as S3),

and the effect of different grouting methods on the bearing capacity of the pile foundation was investigated.

To investigate the load transfer mechanism and distribution of the pile-side frictional resistance of the post-grouting pile during downward compression, ten pairs of strain gauges were arranged at equal intervals along the two sides of each model pile, as shown in Fig. 5. The strain gauges were glued to the surface of the steel bars using epoxy resin. The conductors were fixed to steel bars to prevent physical damage to the strain gauges and conductors during the model pile casting process [24].

A bicycle inner tube was selected to simulate the capsule installed at the end of the pile using the composite post-grouting technology, and a concentric round rubber capsule (10 cm outer diameter and 5 cm inner diameter) was made to bond the steel plate at the pile end. The grouting pipe was buried in advance in the pile body when the model pile was cast. Before the test, the rubber capsule was inflated to check the integrity of the device. A comparison of the pile-end capsules before and after inflation is presented in Fig. 6.

2.5 Experimental Preparation and Testing Process

During the preparation, the model container was placed in the center directly below the loading beam. Vaseline was used on the surface of the inner wall of the model box in advance to reduce the boundary effect [25]. To obtain a uniform distribution of soil in the model foundation, the sandy soil needs to be filled inside the model container in layers. Therefore, it was necessary to mark the scale inside the surface of the container to control the volume of the soil layers. In this study, sand was filled in 5 cm of each layer in the model container to ensure that the unit weight and relative density of the sand were always maintained at 18.2 kN/m^3 and 85.7%, respectively. Malik et al. [26] proposed that the influence zone below the pile toe should be 3.5–5.5d (diameter). Accordingly, when the sand fill height reached 50 cm, which is equals to 5d (diameter), as shown in Fig. 2, the model pile was installed vertically in
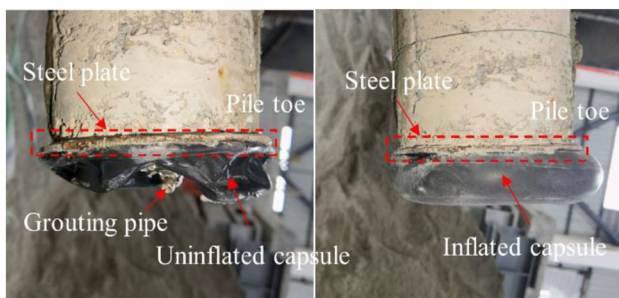
the center of the model container and kept fixed, filling the sand in layers and compacting it until the design position. Additionally, the position of the model pile was fixed during this period and maintained vertically.

After the model is completed and stands for a while [27, 28], the post-grouting test is performed on the pile ends. First, the prepared cement slurry is put into the grouting tank, then the top plate is installed, and all the required preparations before grouting are completed. It should be noted that the grouting pressure is 0.7 MPa, the amount of dry cement powder is 6.25 kg, and the water-cement ratio of the cement slurry is 0.8:1. In the process of the composite post-grouting of pile S3, the slurry is first pressed into the steel plate capsule at the pile bottom through the inlet pipe to expel the air inside the steel plate capsule. Thereafter, the one-way valve at the end of the outlet pipe is closed to start the post-grouting step at the pile bottom after the return of the slurry from the outlet pipe. After the grouting test was completed, the model was left to stand for more than 7 days. After the solidification of the cement, jack and YHD-200 displacement meters were installed, the strain gauge wires were connected to the data acquisition instrument, and the loading was started. Before loading, the ultimate bearing capacity of the model pile was estimated based on existing research methods (e.g., standard calculation methods and numerical analysis). Subsequently, the test adopted a slow maintenance load to gradually apply the static axial load, and the stability criteria and termination loading conditions under all levels of load in the test were based on Chinese standard codes [29]. Moreover, the load applied to the top of the pile increased step by step, and each increase was 10% of the estimated ultimate bearing capacity. The static load generated by the jack was applied to the pile top step-by-step until failure and then unloaded completely to stop the test.

3 Experimental Results

3.1 Load–Settlement Curve

The load–settlement curves of the three piles (i.e., S1, S2, and S3) are shown in Fig. 7. The load–settlement curves of the non-grouting pile, open post-grouting pile, and compound post-grouting pile in the sand have the same variation, showing a steep type. In the early loading stage, the foundation is in the elastic deformation stage, and the settlement increases linearly with increasing load on the pile-top. With a specific value, the settlement increases rapidly, and compression failure is reached. Consequently, the load–settlement curve of the model pile has an inflection point. The load at the inflection point is the ultimate compressive bearing capacity [30]. The bearing capacity
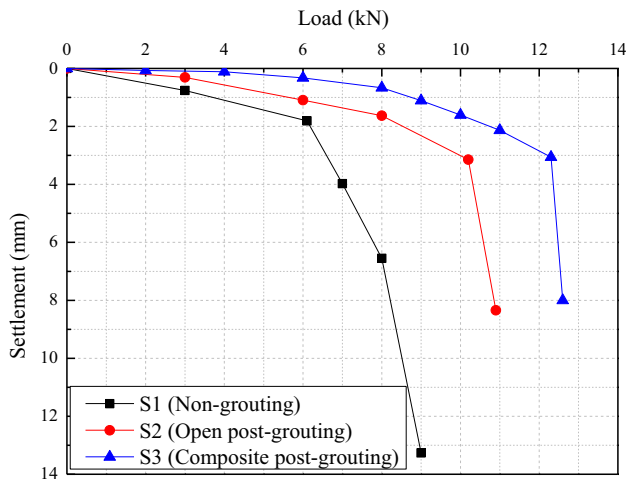

Fig. 6 Comparison of pile-end capsule before and after inflation

Fig. 7 Load–settlement curve

settlement results are summarized in Table 2. When reaching the limit state, the ultimate compressive bearing capacities of the non-grouting pile, open post-grouting pile, and compound post-grouting pile are 6.1, 10.2, and 12.3 kN, respectively. Compared with the non-grouting pile, the ultimate compressive capacity of the model pile increased by 67.2% with open grouting and 101.6% with compound grouting. Therefore, using post-grouting technology at the pile end can significantly enhance the pile's vertical ultimate bearing capacity. It should be highlighted that the improvement effect of the composite post-grouting technology is more evident than that of the open post-grouting technology.

Before the load carrying capacity reaches the limit state, for the equal load, the settlement of a non-grouting pile's top is the largest, whereas the pile top settlement of a composite post-grouting pile is the smallest, and the pile top settlement of an open post-grouting pile is between them. For example, when the load reaches 6.1 kN, the settlement of the open post-grouting pile's top is approximately 61.9% of the non-grouting pile top settlement. In contrast, the settlement of the composite post-grouting pile top was approximately 18.8% of the non-grouting settlement. It was found that the use of post-grouting technology

significantly enhanced the ultimate bearing capacity of the pile foundation and decreased the settlement deformation at the top of the pile. It is noteworthy that composite post-grouting enhances the bearing deformation characteristics of grouted piles in sandy soil more effectively than the commonly used open post-grouting technique. In summary, this composite post-grouting technology is beneficial for shortening the pile length and reducing the construction period and capital investment, while ensuring the requirements of pile-bearing deformation characteristics.
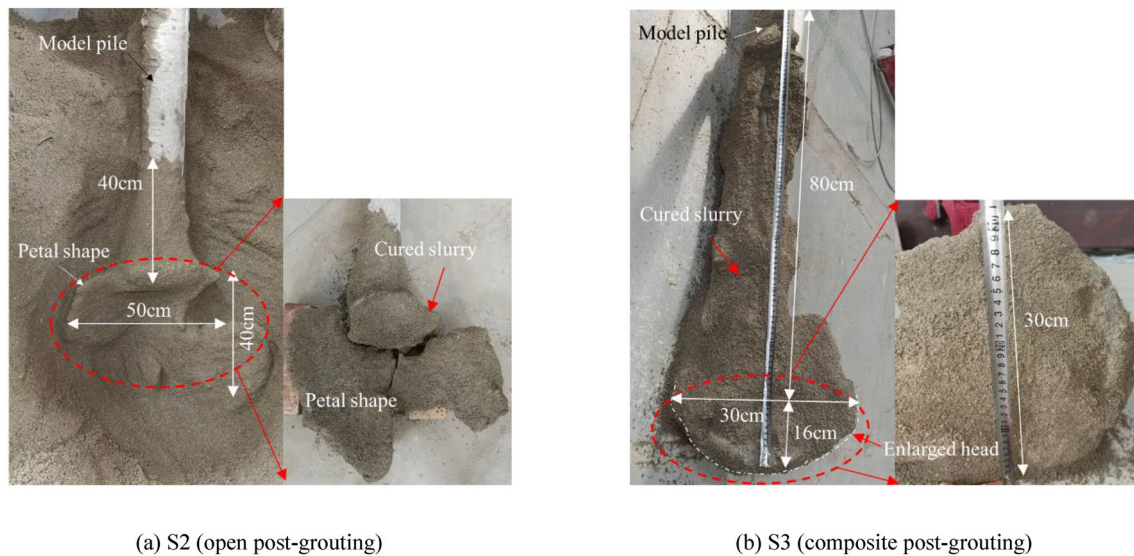
3.2 Cement Curing Performance of Pile-End

To compare the performance of open post-grouting and composite post-grouting on the pile-end reinforcement and effect area, the sandy soil in the model container was cleaned after the model test, and the cement curing performance at the pile-end was observed. Figure 8 shows the pile-end cement curing performance of the open post-grouting and composite post-grouting. For the open post-grouting, the cement cured around the pile end in a petal shape with a length of approximately 20 cm and thickness of 3–4 cm, while there is no grout cured below the center of the pile end. This petal-like cured cement makes the sandy soil denser in the lower 40 cm × 50 cm (depth × width) range of the pile end. In addition, the cement at the pile end flowed upward to the pile side to a height of 40 cm (See Fig. 8a). Although open post-grouting has specific crowding and curing influences on the sandy soil at the end and side of piles, the reinforced area was in the form of an irregular and asymmetric tree-root distribution. Consequently, the integrity and uniformity of the open post-pressure reinforcement are poor, and it is difficult to achieve the reinforcing effect expected by designers.

For the composite post-grouting, the cement at the pile end forms an enlarged head that wraps the pile end tightly and resembles a sphere. Additionally, this enlarged head has a diameter of approximately 30 cm and a height of approximately 16 cm. Except for the enlarged head formed by cement curing, part of the cement slurry flowed upward along the pore space on the pile side, and the maximum upward height could reach 80 cm, as shown in Fig. 8b.

Table 2 Summary of model test results

Pile No	Grouting type	Maximum load (kN)	Maximum settlement (mm)	Ultimate load (kN)	Settlement under ultimate conditions (mm)
S1	Non-grouting	9.0	13.27	6.1	1.81
S2	Open post-grouting	10.9	8.34	10.2	3.15
S3	Composite post-grouting	12.6	8.01	12.3	3.06

(a) S2 (open post-grouting)

(b) S3 (composite post-grouting)

Fig. 8 Comparison of pile-end slurry curing performance

Compared with the open post-grouting, the composite post-grouting cured the pile-end slurry with a broader area, good integrity, and uniformity.

3.3 Axial Force Distribution of the Pile

To investigate the influence of grouting methods on the load transfer of the grouted pile, the pile axial force needs to be solved based on the monitoring data of the strain gauges on the pile's sides. The pile axial force was determined as follows [31]:

$$Q_i = \pi \left(\frac{d}{2}\right)^2 E\varepsilon_i \tag{1}$$

where Q_i is the pile's axial force at section i of pile; d is the pile diameter; E is the pile's elasticity modulus; ε_i is the average measured strain of section i.

Figure 9 illustrates the axial force distribution of the pile. Generally, the axial force without grouting or with different grouting conditions exhibited a consistent pattern of variation. With increasing depth, the axial force gradually decreases. The axial force at the end of the pile is not zero, which indicates the transfer of load to the pile end, which can be treated as the bearing part. For the same depth, the axial force of the pile increased with the load. For non-grouting pile S1, the axial force decays linearly with increasing depth at the same load, as shown in Fig. 9a. For the open post-grouting pile S2, the axial force decays linearly with increasing depth for the same load in the depth range of 0–1.55 m. Subsequently, when the depth is 1.55–2.0 m, the decay rate of the axial pile force with depth increases abruptly, as shown in Fig. 9b. Similarly, for the composite post-grouting pile S3, the axial force

along the pile shaft first decays uniformly with increasing depth, then increases abruptly when the depth reaches 1.35 m and continues to decay linearly toward the bottom of the pile with a more significant decay rate, as shown in Fig. 9c. The axial force decay rate of the pile is an objective reflection of the frictional resistance at the pile side, that is, the greater the decay rate of the axial force, the better is the pile-side frictional resistance. Therefore, for open post-grouting piles and composite post-grouting piles, this decay rate increases at depths of 1.55 m and 1.35 m, respectively. This phenomenon is caused by the cement slurry returned at the pile end, which increases the pile-side friction resistance in the upper part of the pile end, which also verifies the test described in Sect. 3.2.

3.4 Pile-Side Frictional Resistance

The surface friction between the foundation and soil resists a part of the load, which is crucial to the bearing capacity of the pile. Moreover, evaluating the behavior of pile-side friction can help to investigate the proportion of pile end resistance and pile-side friction. According to the axial force distribution shown in Fig. 9, the frictional resistance at the pile side can be expressed as [32, 33]:

$$q_{\mathrm{si}} = \frac{Q_i - Q_{i-1}}{\pi \mathrm{d}l_i} \tag{2}$$

where q_{si} is the average pile-side frictional resistance between section i and section i-1; l_i is the distance between section i and section i-1.

It can be seen from Fig. 10 that the friction resistance of the pile side at the same depth increases with an increase in the pile-top load. For the non-grouting pile S1, the
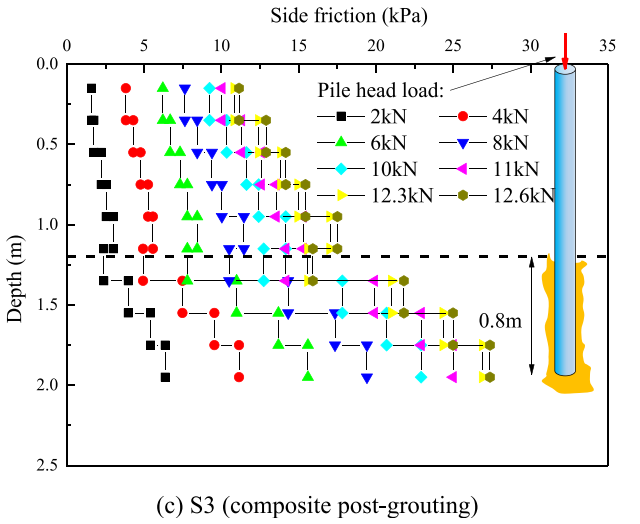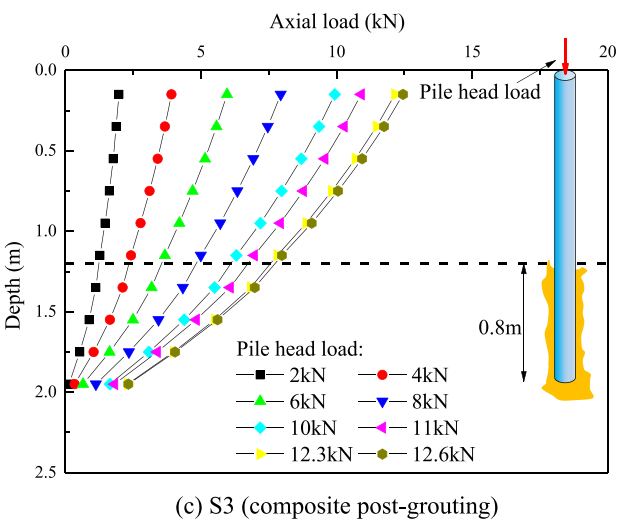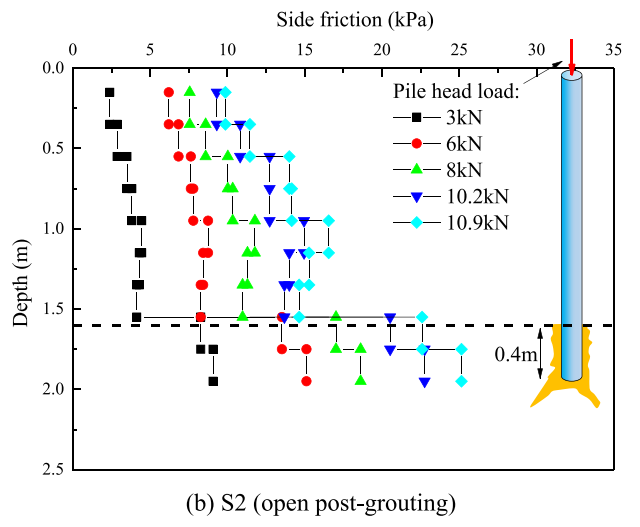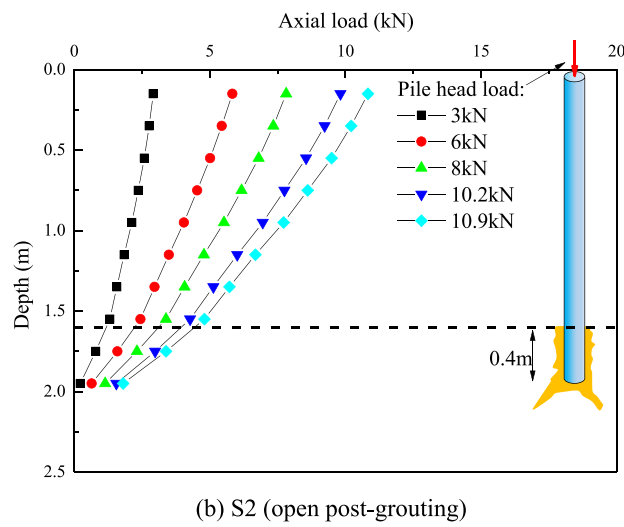
(a) S1 (non-grouting)

(a) S1 (non-grouting)

(b) S2 (open post-grouting)

(b) S2 (open post-grouting)

(c) S3 (composite post-grouting)
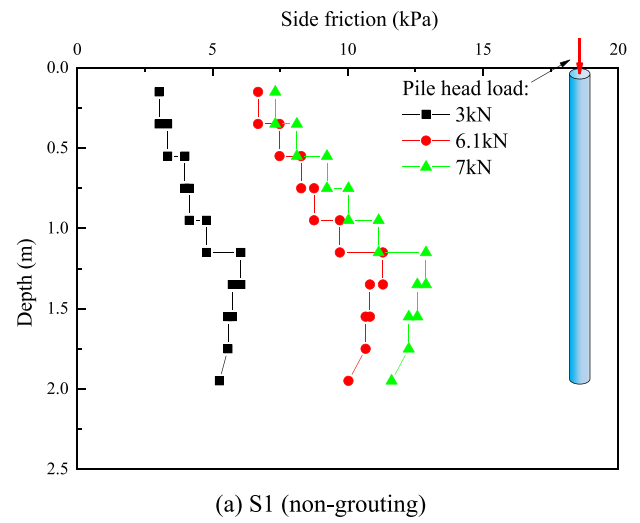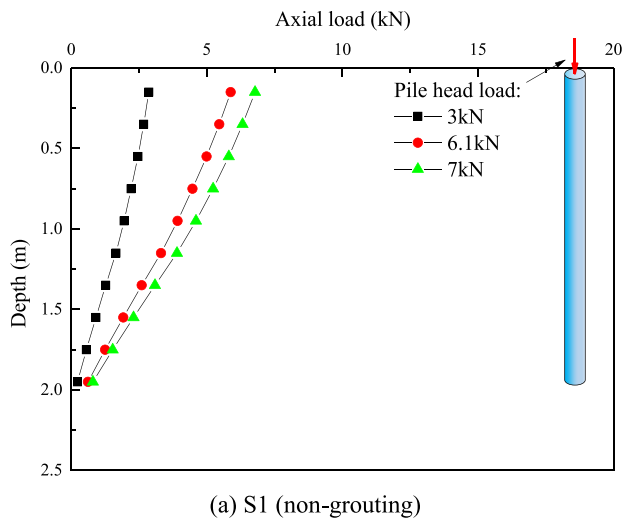

(c) S3 (composite post-grouting)

Fig. 9 Axial force distribution of pile shaft

Fig. 10 Side friction distribution

frictional resistance rises first, drops with increasing depth, and reaches a peak at a depth of 1.35 m in Fig. 10a. For the open post-grouting and the composite post-grouting shown in Fig. 10b and c, the frictional resistance increases and then decreases with the increase in depth. Subsequently, the pile-side frictional resistance in the slurry up-return region increased with depth, and the rate of increase was significantly accelerated. It is evident that the mechanical properties of the soil within the cement slurry up-return region were improved by the upward return and solidification of the pile-side slurry in the S2 and S3 piles before loading. Compared with the S1 pile (i.e., non-grouting), the average pile-side frictional resistance within the pile-side slurry up-return area of the S2 (i.e., open post-grouting) and S3 (i.e., composite post-grouting) piles at the ultimate state was improved by 109.3% and 129.3%, respectively. Therefore, open post-grouting and composite post-grouting technologies can improve the pile-end resistance and increase the pile-side friction resistance of the upper part of the pile end. In contrast, composite post-grouting has a greater increase in pile-side friction resistance and a wider range of influence.
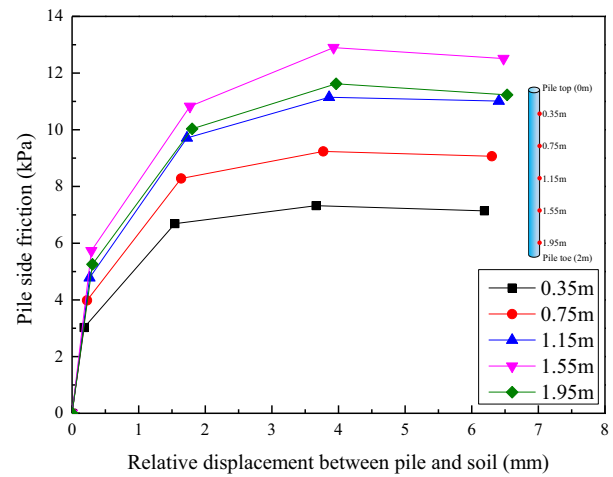
3.5 Relative Displacement of Pile-Soil

The pile-soil relative displacement is an important factor that affects the lateral frictional resistance of the pile and the bearing capacity performance of the post-grouting pile. The relative displacement of the pile-soil is described using Eq. (3) [34]:

$$s_{si} = s_t - \sum_{j=1}^{i} \frac{l_j}{2}\left(\varepsilon_j + \varepsilon_{j+1}\right) \tag{3}$$

where s_{si} is the relative pile-soil displacement at section i; s_t is the pile-top displacement; ε_j, ε_{j+1} are the strains at sections j and $j + 1$, respectively, and l_j is the soil thickness of the jth layer of soil.

Figure 11 shows the curves of the friction resistance and relative displacement. For S1 (i.e., non-grouting), S2 (i.e., open post-grouting), and S3 (i.e., composite post-grouting) piles, the pile-side frictional resistance at different burial depths rises with the growth of pile-soil relative displacement, and the increment decreases gradually. When the test pile was about to reach the failure state, the side friction of the pile was the highest. Subsequently, the pile-side resistance decreases slightly with increasing relative displacement, and the pile-side soil softens. Compared with S1 (i.e., non-grouting), when the pile-soil relative displacement is equal, the pile-side frictional resistance of S3 (i.e., composite post-grouting) is more significant than that of S2 (i.e., open post-grouting), and both are greater than that of S1 (i.e., non-grouting). Moreover, when the test pile

(a) S1 (non-grouting)
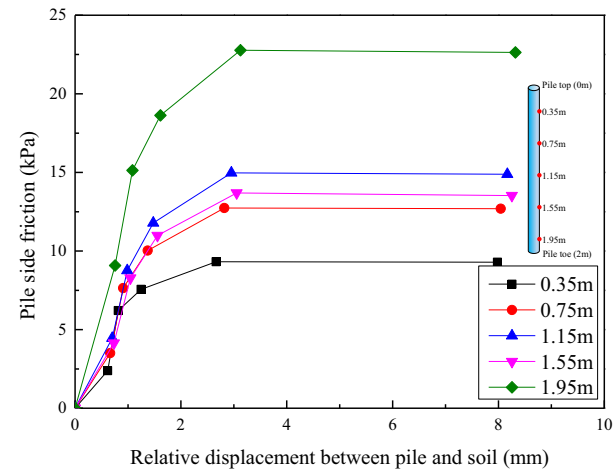
(b) S2 (open post-grouting)
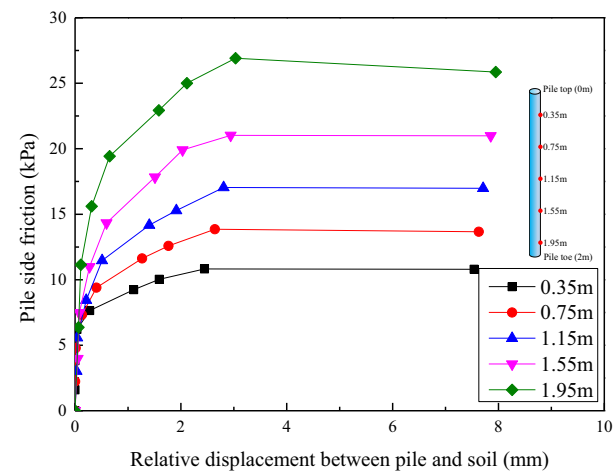
(c) S3 (composite post-grouting)

Fig. 11 Relationship between pile-side frictional resistance and pile-soil relative displacement

reached failure, the pile-soil relative displacement of S3 was smaller than that of S2, and both were less than that of S1. It is indicated that the cement slurry within the pile tip significantly changes the physical and mechanical characteristics of the pile-side soil and effectively increases the shear strength of the soil in the return area, which is more evident with the composite post-grouting. The softening of the pile-side frictional resistance of S3 lags behind that of S2, indicating that after the composite post-grouting, the curing range of the grouted slurry at the pile end is effectively and reliably controlled owing to the restraint of the annular steel plate capsule at the pile bottom, thus improving the load-bearing deformation capacity of the foundation.

3.6 Pile-End Resistance

The pile's bearing capacity has two parts: the frictional resistance of the pile side and the resistance of the pile end. Hence, the pile-end resistance is also an essential factor affecting the bearing capacity. Li et al. [35] proposed a hyperbolic model to describe the relationship between pile toe stress and pile base displacement. In this study, the relationship between the pile-end displacement and pile-end stress of S1-S3 is fitted by the hyperbolic function, as shown in Fig. 12, as presented in Eq. (4):

$$q_b = \frac{s_b}{c \cdot s_b + d} \tag{4}$$

where q_b is the pile-end stress; s_b is the pile-end displacement; c and d are the hyperbolic model parameters.

From Fig. 12, the relationship curve between pile-end displacement and resistance is hardened and can be better fitted using a hyperbolic function ($R^2 = 0.907$–0.994). When the displacement is the same, the resistance of the
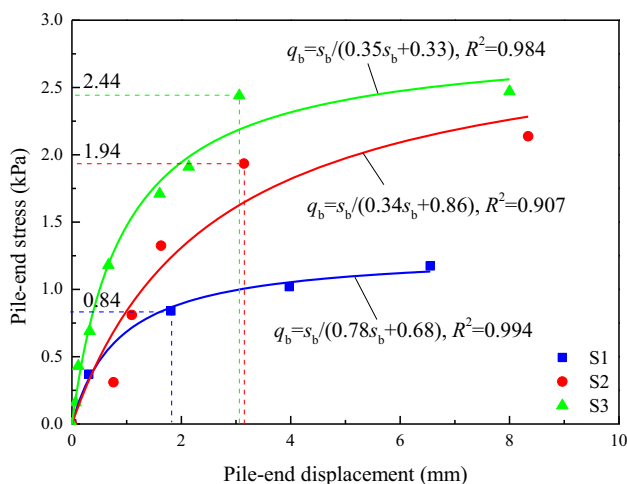
pile end is $S1 < S2 < S3$, which indicates that after adopting the composite post-grouting technology, the hollow steel plate capsule can confine and fix the grouted slurry in the pile end capsule, forming a cement extrusion expanding head and increasing the support area of the pile end, which effectively squeezes the ground around the pile bottom. The open grouting before and after the closed grouting of the pile end can infiltrate or split the grouted slurry on the soil around the pile bottom, and the slurry is cemented and cured in the ground layer at the pile end to substantially improve the foundation strength. Compared with the S1 non-grouting pile, the pile-end resistance of S2 with open post-grouting and S3 with composite post-grouting at the ultimate condition increased by 2.3 (1.94/0.84) times and 2.9 (2.44/0.84) times, respectively.

The relationship between the pile-end resistance bearing ratio (defined as the ratio of the end resistance to the corresponding load of the pile-top) and the pile-top load is shown in Fig. 13. With the gaining of pile top load, the end resistance ratios of S1 (i.e., non-grouting), S2 (i.e., open post-grouting), and S3 (i.e., composite post-grouting) piles increased linearly. With the increasing pile top load, the end resistance ratio increased from 12.3% to 13.8%, corresponding to a pile top load of 3–6.1 kN for the S1 pile, from 10.3% to 19.0%, corresponding to a pile top load of 3–10.2 kN for the S2 pile, and from 8.0% to 19.8%, corresponding to a pile top load of 2–12.3 kN for the S3 pile. When reaching the ultimate state, there is a larger end-resistance sharing ratio of the S3 pile and pile top load than that of the S2 and S1 piles. The ultimate state pile-end resistance of S3 is 2.44 kN, which is 190.5% and 25.8% higher than that of test piles S1 (0.84 kN) and S2 (1.94 kN), respectively. Thus, the composite post-grouting technique leads to an increase in bearing capacity and is superior to the open post-pressure technique in terms of
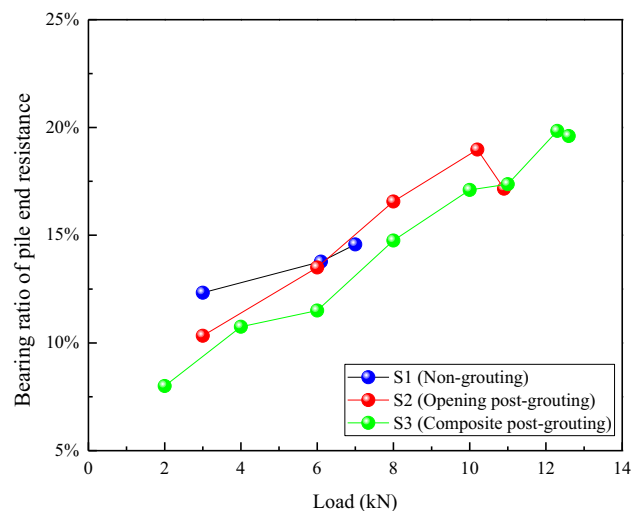

Fig. 12 The relationship curve between displacement and stress of the pile-end

Fig. 13 Bearing ratio of pile tip resistance of S1–S3

pile-end bearing capacity under the same conditions. When S2 and S3 reach the ultimate state, the end resistance sharing ratio is very similar, which is caused by the fact that the slurry returned on the S3 pile end is more extensive than the slurry returned on the S2 pile end to get better wrapping on the pile body. Therefore, compared with the open post-grouting technique, the composite post-grouting technique increases the pile-side frictional resistance in the pile-end slurry up-return zone, thereby affecting the proportion of the end resistance.

4 Conclusions

In this study, static load compressive tests of three model piles treated with different post-grouting techniques were performed using indoor model tests, and the load–settlement curve, cement slurry curing performance, pile axial force distribution, pile-side frictional resistance, pile-soil relative displacement, and pile-end resistance characteristics of the model piles were investigated. The following conclusions were drawn:

1. The load–displacement curves of the non-grouting piles, open post-grouting piles, and composite post-grouting piles in sandy soil showed the same pattern of steep variation. Compared with the non-grouting pile, the ultimate compressive bearing capacity was enhanced by 67.2% with open post-grouting and by 101.6% with composite post-pressure at the pile end. Compared with the commonly used open post-grouting technique, the composite post-grouting technique significantly enhances the bearing deformation characteristics in sandy soil.

2. For open post-grouting, the cement slurry around the pile-end cures in a petal shape (length of approximately $2d$, thickness of $0.3 \sim 0.4d$), while no slurry cures below the center of the pile-end. In contrast, composite post-grouting allows the slurry at the pile end to cure to form an enlarged head that wraps the pile end tightly and resembles a sphere. Furthermore, the composite post-grouting allows the pile-end slurry to return up to approximately twice the curing height of the open post-grouting, which has good wrapping, integrity, and uniformity.

3. Compared with the S1 pile without grouting, the average pile-side frictional resistance in the slurry upward return area of S2 with open post-grouting and S3 with composite post-grouting at the ultimate condition increased by 109.3% and 129.3%, respectively. In addition, the composite post-grouting technology enhances the pile-end resistance and increases the pile-side friction resistance at the upper part of the

pile-end, which has more improvement and a wider influence region.

4. The relationship curve between the pile-end displacement and pile-end stress is hardened and can be better represented by a hyperbolic function. Compared with the S1 pile without grouting, the pile-end resistance of S2 with open post-grouting and S3 with composite post-grouting at the ultimate state is increased by 2.3 times and 2.9 times, respectively. In contrast, composite post-grouting technology enlarges the bearing area and greatly increases the bearing capacity of the pile tip.

Data availability All data, models, or code that support the findings of this study are available from the corresponding author upon reasonable request.

Declarations

Conflict of interest The authors declared that there is no conflict of interest.

References

1. Dai GL, Gong WM, Zhao XL, Zhou XQ (2010) Static testing of pile-base post-grouting piles of the Suramadu bridge. Geotech Test J 34(1):34–49. https://doi.org/10.1520/GTJ102926
2. Thiyyakkandi S, McVay M, Lai P (2014) Experimental group behavior of grouted deep foundations. Geotech Test J 37(4):621–638. https://doi.org/10.1520/GTJ20130144
3. Safaqah O, Bittner R, Zhang X (2007) Post-grouting of drilled shaft tips on the Sutong Bridge: a case history. In: Contemporary issues in deep foundations, pp. 1–10
4. Rollins KM, Adsero ME, Dan AB (2009) Jet grouting to increase lateral resistance of pile group in soft clay. Proceedings of International Foundation Congress and Equipment Expo, Orlando, pp. 265–272
5. Zhou JJ, Yu JL, Gong XN, Naggar MHE, Zhang RH (2021) Field study on the behavior of pre-bored grouted planted pile with enlarged grout base. Acta Geotech. https://doi.org/10.1007/s11440-021-01208-7
6. Ghazali FM, Sotiropoulos E, Mansour OA (1988) Large-diameter bored and grouted piles in marine sediments of the red sea. Can Geotech J 25:826–831. https://doi.org/10.1139/t88-090
7. Nguyen MH, Fellenius BH (2015) Bidirectional cell tests on non-grouted and grouted large-diameter bored piles. J GeoEng Sci 2(3):105–117. https://doi.org/10.3233/JGS-140025
8. Xing HF, Liu LL, Luo Y, Ye GB (2019) Effects of construction technology on bearing behaviors of rock-socketed bored piles as bridge foundations. J Bridge Eng 24(4):05019002. https://doi.org/10.1061/(ASCE)BE.1943-5592.0001368

9. Zhou YL, Wang X, Zhang YJ, Zhang XH, Gao YG, Ye YG (2022) Composite post grouting at pile tip and bearing characteristics of cast-in-place pile foundation. Chin J Geotech Eng 44(10):1864–1872 (**in Chinese**)

10. Bruce DA (1986) Enhancing the performance of large diameter piles by grouting. Ground Eng 19(4):9–15

11. Sherwood DE, Mitchell JM (1989) Based grouted piles in Thanet sands. Proceedings of 3rd International conference on Piling and Deep Foundations, London, pp. 463–472

12. Ruiz ME, Pando MA (2009) Load transfer mechanisms of tip post-grouted drilled shafts in sand. Proceedings of International Foundation Congress and Equipment Expo: Contemporary Topics in Deep Foundation, pp. 23–30

13. Thiyyakkandi S (2013) Study of grouted deep foundations in cohesionless soil. Ph.D Thesis, University of Florida

14. Thiyyakkandi S, McVay M, Bloomquist D, Lai P (2013) Measured and predicted response of a new jetted and grouted precast pile with membranes in cohesionless soil. J Geotech Geoenviron Eng 139(8):1334–1345. https://doi.org/10.1061/(ASCE)GT.1943-5606.0000860

15. Youn H, Tonon R (2010) Numerical analysis on post-grouted drilled shafts: a case study at the brazo river bridge TX. Comput Geotech 37(4):456–465. https://doi.org/10.1016/j.compgeo.2010.01.005

16. Fang K, Zhang Z, Zhang Q, Liu XW (2014) Prestressing effect evaluation for a grouted shaft: a case study. Proc Inst Civ Eng Geotech Eng 167(3):253–261. https://doi.org/10.1680/geng.11.00090

17. Xu MJ, Zhang FY, Ni PP, Mei GX (2022) Load-settlement behaviour of membrane-confined grouted pile: experimental and analytical study. Acta Geotech. https://doi.org/10.1007/s11440-022-01711-5

18. Wan ZH, Dai GL, Gong WM (2019) Field study on post-grouting effects of cast-in-place bored piles in extra-thick fine sand layers. Acta Geotech 14:1357–1377. https://doi.org/10.1007/s11440-018-0741-7

19. Wang JC, Wang XW, Liu TF, Ye AJ (2022) Seismic uplift behavior and energy dissipation mechanism of scoured bridge pile-group foundations: Quasi-static test and numerical analysis. Ocean Eng 266:113172. https://doi.org/10.1016/j.oceaneng.2022.113172

20. Buckingham E (1914) On physically similar systems; illustrations of the use of dimensional equations. Phys Rev 4(4):345–376. https://doi.org/10.1103/physrev.4.345

21. Garnier J, Gaudin C, Springman SM, Culligan PJ, Thorel L (2007) Catalogue of scaling laws and similitude questions in geotechnical centrifuge modeling. Int J Phys Model Geotech 7(3):1–23. https://doi.org/10.13140/2.1.1615.3281

22. Craig WH (1984) Installation studies for model piles. Proceedings of symposium on the application of centrifuge modeling to geotechnical design, Manchester, pp. 440–455

23. Ovesen NK (1979) The use of physical models in design: the scaling law relationships. Proceedings of 7th European Conference on Soil Mechanics and Foundation Engineering, Brighton, 4: 318–323

24. Sawada K, Takemura J (2014) Centrifuge model tests on piled raft foundation in sand subjected to lateral and moment loads. Soil Found 54(2):126–140. https://doi.org/10.1016/j.sandf.2014.02.005

25. Wang QK, Ma JL, Ji YK, Cao S (2021) Calculation method and influencing factors of uplift bearing capacity of rock-socketed pedestal pile. Arab J Geosci 14(4):243. https://doi.org/10.1007/s12517-021-06567-9

26. Malik AA, Kuwano J, Tachibana S, Maejima T (2017) End bearing capacity comparison of screw pile with straight pipe pile under similar ground conditions. Acta Geotech 12:415–428. https://doi.org/10.1007/s11440-016-0482-4

27. Li WD, Deng LJ (2019) Axial load tests and numerical modeling of single-helix piles in cohesive and cohesionless soil. Acta Geotech 14:461–475. https://doi.org/10.1007/s11440-018-0669-y

28. Wan ZH, Dai GL, Gong WM (2022) Study on the response of postside-grouted piles subjected to lateral loading in calcareous sand. Acta Geotech 17:3099–3115. https://doi.org/10.1007/s11440-021-01392-6

29. JGJ 106-2014 (2014) Technical code for testing of building foundation piles. JGJ 106-2014, Ministry of Construction of the People's Republic of China, Beijing, China. (in Chinese)

30. JGJ 94-2008 (2008) Technical code for building pile foundations. JGJ 94-2008, Ministry of Construction of the People's Republic of China, Beijing, China. (in Chinese)

31. Xu MJ, Ni PP, Mei GX, Zhao YL (2018) Load-settlement behaviour of bored piles with loose sediments at the pile tip: experimental, numerical and analytical study. Comput Geotech 102:92–101. https://doi.org/10.1016/j.compgeo.2018.06.010

32. Xing HF, Zhang Z, Meng MH, Luo Y, Ye GB (2014) Centrifuge tests of superlarge-diameter rock-socketed piles and their bearing characteristics. J Bridge Eng ASCE 19(6):04014010. https://doi.org/10.1061/(ASCE)BE.1943-5592.0000582

33. Wang QK, Hu ZB, Ji YK, Ma JL, Chen WL (2022) Model test of rock-socketed pile under axial and oblique tension loading in combined composite ground. Int J Geomech 22(10):04022182. https://doi.org/10.1061/(ASCE)GM.1943-5622.0002532

34. Wang QK, Ma JL, Wang MT, Ji YK (2021) Field test on uplift bearing characteristics of transmission tower foundation in mountainous areas of western China. Environ Earth Sci 80(22):745. https://doi.org/10.1007/s12665-021-09851-9

35. Li SC, Zhang Q, Zhang QQ, Li LP (2016) Field and theoretical study of the response of super-long bored pile subjected to compressive load. Mar Georesour Geotechnol 34:71–78. https://doi.org/10.1080/1064119X.2014.958883